contrast to the analogous reactions of CHD_3 (v_1 = 1) with F and O(^{3}P) atoms (*9*, *10*). In retrospect, this implication may not be too surprising. It has been demonstrated (*22*, *29*) that in the ground-state Cl + CHD_3 reaction, the product angular distribution essentially mirrors the opacity function (the reaction probability as a function of impact parameters) in a one-to-one correspondent manner [see figures 2 and 5 of (*22*)]. In accounting for enforcement of such a mirror-like correspondence, a rather weak anisotropic PES in the entrance valley could have been inferred. The structure of the transition state is product-like, and thus the reaction barrier is recessed in the exit valley. Upon vibrational excitation of CHD_3(v_1 = 1), the elongation of the C-H bond can enlarge the range of attack angles at the reaction barrier, thereby increasing the reaction probability at fixed impact parameters, but the resulting anisotropic interactions may not extend into the entrance valley far enough to appreciably steer the prealigned reagents.

References and Notes

1. F. F. Crim, *Proc. Natl. Acad. Sci. U.S.A.* **105**, 12654 (2008).
2. W. L. Hase, *Science* **266**, 998 (1994).
3. D. C. Clary, *Annu. Rev. Phys. Chem.* **41**, 61 (1990).
4. A. J. Orr-Ewing, R. N. Zare, *Annu. Rev. Phys. Chem.* **45**, 315 (1994).
5. D. Skouteris *et al*., *Science* **286**, 1713 (1999).
6. R. D. Levine, *J. Phys. Chem.* **94**, 8872 (1990).
7. A. J. Alexander, M. Brouard, K. S. Kalogerakis, J. P. Simons, *Chem. Soc. Rev.* **27**, 405 (1998).
8. B. L. Yoder, R. Bisson, R. D. Beck, *Science* **329**, 553 (2010).
9. W. Zhang, H. Kawamata, K. Liu, *Science* **325**, 303 (2009).
10. F. Wang, K. Liu, *Chem. Sci.* **1**, 126 (2010).
11. G. Czakó, J. M. Bowman, *J. Am. Chem. Soc.* **131**, 17534 (2009).
12. The contrasting behaviors of O and F can also be qualitatively rationalized from the transition-state theory perspective. The transition state in F + CHD_3 possesses a reactant-like structure, and thus a stretched or compressed C-H bond of CHD_3 deviates from the transition-state structure, disfavoring the reaction. By contrast, ab initio calculations predicted that in O(^{3}P) + CHD_3, both the breaking C-H bond and forming O-H bond are elongated. Excitation of the C-H bond of CHD_3 therefore helps attain the transition-state structure.
13. W. R. Simpson, T. P. Rakitzis, S. A. Kandel, A. J. Orr-Ewing, R. N. Zare, *J. Chem. Phys.* **103**, 7313 (1995).
14. W. T. Duncan, T. N. Truong, *J. Chem. Phys.* **103**, 9642 (1995).
15. J. C. Corchado, D. G. Truhlar, J. Espinosa-Garcia, *J. Chem. Phys.* **112**, 9375 (2000).
16. S. Yan, Y.-T. Wu, B. Zhang, X.-F. Yue, K. Liu, *Science* **316**, 1723 (2007).
17. S. Yan, Y.-T. Wu, K. Liu, *Proc. Natl. Acad. Sci. U.S.A.* **105**, 12667 (2008).
18. J. J. Lin, J. Zhou, W. Shiu, K. Liu, *Rev. Sci. Instrum.* **74**, 2495 (2003).
19. J. J. Lin, J. Zhou, W. Shiu, K. Liu, *Science* **300**, 966 (2003).
20. O. N. Ulenikov *et al*., *Mol. Phys.* **108**, 1209 (2010).
21. Magic angle imaging serves two purposes. First, at this polarization angle, the approaching Cl atom encounters a practically unpolarized CHD_3(v_1 = 1, j = 1) reagent. Previously, when we prepared CHD_3(v_1 = 1) in the source chamber (*16*, *17*), the excited reagents traveled for >100 μs before reacting, which we presumed was long enough to depolarize initially aligned CHD_3(v_1 = 1) molecules by hyperfine interactions. Indeed, the results from the acquired α_M image agree broadly with the previous findings. Second, the signals from the stretch-excited reagents under the three polarization angles are related by ($I_{//}$ + 2$I_{\perp}$) = 3Iα_M, which provides a stringent check (within ±1% in this work) of the consistency of the data.
22. G. Nyman, J. Zhou, B. Zhang, K. Liu, *Isr. J. Chem.* **47**, 1 (2007).
23. R. N. Zare, *Ber. Bunsenges. Phys. Chem* **86**, 422 (1982).
24. R. Altkorn, R. N. Zare, C. H. Greene, *Mol. Phys.* **55**, 1 (1985).
25. R. D. Levine, R. B. Bernstein, *Molecular Reaction Dynamics and Chemical Reactivity* (Oxford Univ. Press, Oxford, 1987).
26. In an optically aligned (not oriented) CHD_3 molecule, the H atom of the aligned C-H bond can point either toward or away from the approaching Cl atom; thus, no distinction of the head-versus-tail dynamics can be made.
27. In a direct reaction, the forward-scattered product is normally associated with large–impact parameter collisions, for which there is a purely kinematic smearing of the alignment effect even for a perfectly aligned reagent (*30*).
28. R. Martínez, M. González, P. Defazio, C. Petrongolo, *J. Chem. Phys.* **127**, 104302 (2007).
29. J. Zhou, B. Zhang, J. J. Lin, K. Liu, *Mol. Phys.* **103**, 1757 (2005).
30. I. Schetchter, R. D. Levine, *J. Chem. Soc. Faraday Trans. II* **85**, 1059 (1989).

31. We are indebted to S. Yan for earlier attempts of this project and to J. Lam for help with the experiment. This work was supported by National Science Council (NSC-99-2113-M-011-016), Academia Sinica, and the Air Force Office of Scientific Research (AOARD-10-4034).

Supporting Online Material

www.sciencemag.org/cgi/content/full/331/6019/900/DC1
Figs. S1 to S5
Tables S1 and S2
References

29 October 2010; accepted 13 January 2011
10.1126/science.1199771

The Magnitude and Duration of Late Ordovician–Early Silurian Glaciation

Seth Finnegan,[1]* Kristin Bergmann,[1] John M. Eiler,[1] David S. Jones,[2] David A. Fike,[2] Ian Eisenman,[1,3] Nigel C. Hughes,[4] Aradhna K. Tripati,[1,5] Woodward W. Fischer[1]

Understanding ancient climate changes is hampered by the inability to disentangle trends in ocean temperature from trends in continental ice volume. We used carbonate "clumped" isotope paleothermometry to constrain ocean temperatures, and thereby estimate ice volumes, through the Late Ordovician–Early Silurian glaciation. We find tropical ocean temperatures of 32° to 37°C except for short-lived cooling by ~5°C during the final Ordovician stage. Evidence for ice sheets spans much of the study interval, but the cooling pulse coincided with a glacial maximum during which ice volumes likely equaled or exceeded those of the last (Pleistocene) glacial maximum. This cooling also coincided with a large perturbation of the carbon cycle and the Late Ordovician mass extinction.

Earth history is punctuated by glacial episodes that vary widely in their magnitude and duration (*1*), as well as in their effects on global biodiversity (*2*). Far more is known about the most recent glacial age in the Pleistocene than about older glacial episodes. The Late Ordovician–Early Silurian glaciation of the southern supercontinent of Gondwana (Fig. 1A) is unusual because it occurred during a period when atmospheric partial pressure of CO_2 (pCO_2) was generally higher [perhaps 8 to 16 times higher (*3*)] than today's pCO_2, was short-lived compared to subsequent Gondwanan glaciations (*1*), and is the only glacial episode that appears to have coincided with a major mass extinction of marine life (*4*) (Fig. 1B). These observations have led to suggestions that the Late Ordovician–Early Silurian icehouse represents a climate mode distinct from more recent glaciations (*5*), but fundamental questions about the event are still largely unresolved: Estimates of peak ice sheet volume range from ~50 to more than 250 million km^3 (*6*) (Fig. 1A), estimates of its duration range from 35 million years (*1*) to less than 1 million years (*5*) (Fig. 1B), and it is unclear how much sea surface temperatures (SSTs) cooled in the tropical environments that hosted much of Late Ordovician biodiversity (*7*–*9*).

These uncertainties persist because few climate proxies can be reliably applied to Paleozoic rocks. Oxygen isotope ratios ($\delta^{18}O$) in well-preserved marine carbonate and phosphate minerals provide a useful proxy and have been widely applied in Paleozoic climate reconstruction (*5*, *7*, *8*) but suffer a fundamental limitation: The $\delta^{18}O$ value of a mineral is influenced by both the temperature and the isotopic composition of the water reservoir from which it precipitates ($\delta^{18}O_{water}$). Consequently, without independent constraints on one or the other of these variables, interpreting $\delta^{18}O$ trends in the stratigraphic record poses an underdetermined problem. This issue has been addressed for the Pleistocene last glacial maximum (LGM)—for example, using sediment porewater profiles (*10*)—but remains largely unresolved for older glaciations.

We used carbonate clumped isotope paleothermometry (*11*, *12*) to constrain the precipitation temperatures of a suite of Late Ordovician–Early Silurian carbonates. This approach measures the state of ordering of heavy isotopes (Δ_{47}) in carbonate minerals and is independent of the

[1]Division of Geological and Planetary Sciences, California Institute of Technology, Pasadena, CA 91125, USA. [2]Department of Earth and Planetary Sciences, Washington University, St. Louis, MO 63130, USA. [3]Department of Atmospheric Sciences, University of Washington, Seattle, WA 98195, USA. [4]Department of Earth Sciences, University of California, Riverside, CA 92521, USA. [5]Department of Earth and Space Sciences and Department of Atmospheric and Oceanic Sciences, Institute of Geophysics and Planetary Physics, University of California, Los Angeles, CA 90095, USA.

*To whom correspondence should be addressed. E-mail: sethf@caltech.edu

isotopic composition of water from which the minerals grew. Combination of this approach with conventional carbonate-water oxygen isotope paleothermometry thus provides a means for untangling trends in reservoir composition from those in temperature. To minimize the effects of burial diagenesis, we examined exceptionally fossiliferous and well-studied successions in the U.S. midcontinent and on Anticosti Island, Québec, Canada (*13*) (Fig. 1A and fig. S1), which have experienced relatively little sedimentary burial. To assay the quality of our proxy measurements, we sampled fossils from several taxonomic groups and surrounding sediments from a broad range of lithotypes and across a large range of preservation states to characterize diagenesis and vital effects (*13*) (figs. S2 and S3).

There is no evidence of a systematic burial overprint on Δ_{47} values in our data set. Similar ranges are recorded in the Vauréal Formation and the Jupiter Formation (Fig. 2A) (*12*) despite ~500 m of intervening strata in the Anticosti Basin (fig. S1). The highest Δ_{47} values (lowest temperatures) on Anticosti are not observed in the stratigraphically highest samples but rather in samples from the middle of the stratigraphic column. To confirm that Δ_{47} does capture known postdepositional thermal gradients, we sampled micritic carbonates from the Vauréal Formation that are intruded by a Jurassic-aged dike. Δ_{47} values immediately adjacent to the dike are the lowest in our entire data set, corresponding to precipitation temperatures exceeding 230°C, but inferred temperatures fall to 39°C within 14 m of the dike-country rock contact (fig. S4).

Δ_{47} values of skeletal carbonates range from 0.631 to 0.501 (Fig. 2 and table S1), corresponding to a temperature range from 28° to 64°C. This range implies a mixture of plausibly primary and diagenetically altered phases, the latter being typically depleted in both Δ_{47} and $\delta^{18}O$ (fig. S5). Because diagenetic recrystallization of calcite tends to deplete Sr and enrich Mn and Fe (*14*, *15*), we evaluated concentrations of these metals in a large and representative subset of our samples (*13*) (figs. S6 to S8). Most samples fall within the "well-preserved" compositional range identified by previous studies (fig. S6), but there is a strong relationship between the first principal component (PC1) of trace metal concentrations and Δ_{47}: High PC1 values (low Sr and high Mn and Fe, fig. S7) are associated with higher precipitation temperatures and in many cases with textural evidence of diagenetic alteration (Fig. 2B). The highest Δ_{47} value and lowest PC1 value associated with texturally altered samples are 0.589 and –0.285, respectively. We therefore excluded all samples that fall outside this range from our reconstructions of ocean temperature and chemistry (Fig. 2B). We included samples that were not evaluated for trace metal concentration but that have Δ_{47} values higher than 0.589, but similar trends result if these samples are also excluded (fig. S9). Even the best-preserved samples likely contain small amounts of dispersed recrystallized phases that cannot easily be avoided given the large sample sizes required for adequately precise measurement of Δ_{47}. Our temperature reconstructions should therefore be viewed as maximal SST estimates, and we base trend lines on the lowest-temperature samples from each stratigraphic interval.

Reconstructed temperatures are nearly indistinguishable from each other and consistent with a narrow range from 32° to 37°C throughout most of the ~20 million years covered by our time series (Fig. 3A). SSTs in this range rarely occur in the modern tropics, but a variety of proxies record similar temperatures during Mesozoic–early Cenozoic greenhouse intervals (*16*–*18*), during which atmospheric pCO_2 is inferred in some reconstructions to have exceeded five times present atmospheric levels (*3*). Temperatures below this range (28° to 31°C) occur only in samples from the Laframboise Member of the Ellis Bay Formation on Anticosti Island. This Hirnantian-aged unit (*13*) records a major drop in sea level (*19*, *20*) and a large positive carbon isotope excursion (*19*); both are recognized globally in other sedimentary successions (*4*, *20*). The best preserved of these successions also record exceptionally enriched $\delta^{18}O$ values [–2 per mil (‰) to 0‰ Vienna Pee Dee belemnite (VPDB)] during Hirnantian time (*8*, *20*, *21*), as do our Laframboise Member samples (Fig. 3B and table S1). $\delta^{18}O$ values preceding and following the Hirnantian peak are lighter but still enriched relative to the ~–5‰ (VPDB) baseline values that characterize the beginning and end of the time series (Fig. 3B). Well-preserved brachiopods and trilobites could not be extracted from the Laframboise Member, and hence our data from the Hirnantian maximum are derived exclusively from rugose corals. Δ_{47} is not known to be subject to disequilibrium vital effects among modern taxa (*11*), but such effects cannot be ruled out and there remains uncertainty regarding the possibility of a vital effect on $\delta^{18}O$ in rugose corals (*13*). However, our Hirnantian $\delta^{18}O$ values are similar to those recorded by brachiopods in contemporaneous sections (*5*, *8*, *20*, *21*), and the

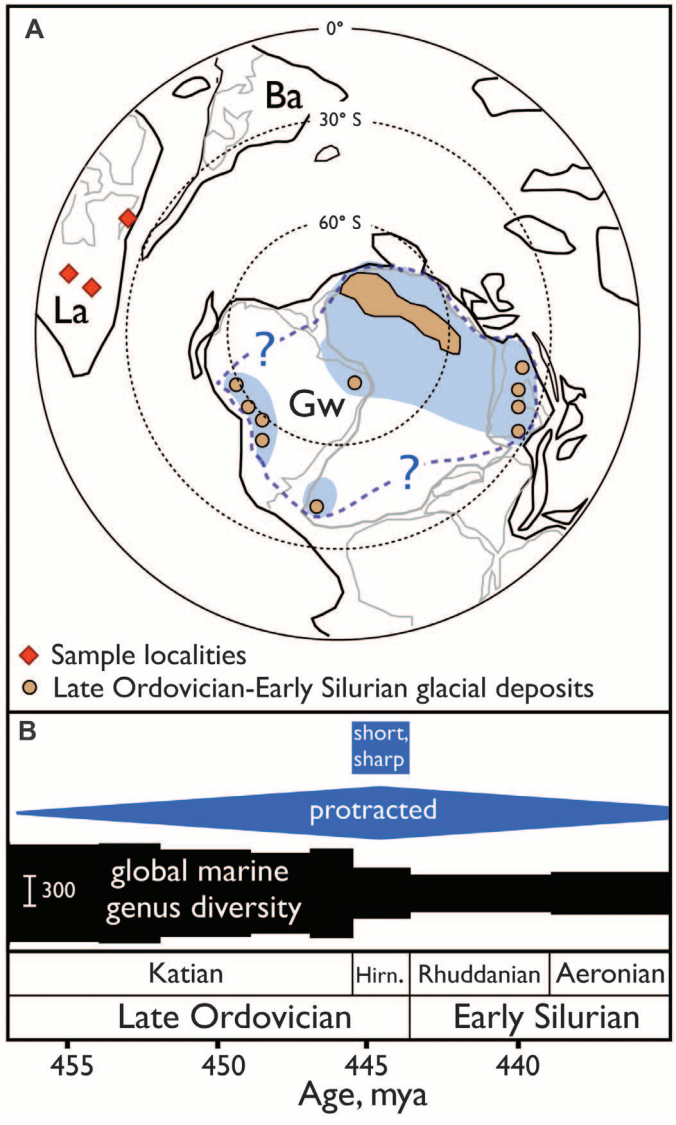

Fig. 1. (**A**) South polar view of a simplified Late Ordovician paleogeographic reconstruction (*27*), indicating the positions of Late Ordovician to Early Silurian–aged glacial deposits in Gondwana (Gw, tan solid circles and areas) and of the Laurentian (La) localities sampled for this study (red diamonds). Ba indicates Baltica. Two possible reconstructions of the Gondwanan ice sheet (*6*) are shown: a minimal, discontinuous reconstruction (light blue shading) and a maximal continent-spanning reconstruction (dashed blue outline). (**B**) Hypotheses regarding the duration of the icehouse interval: short and sharp, restricted largely or entirely to the Hirnantian (Hirn.) stage lasting as little as 500,000 years (*5*), and protracted, with a peak in the Hirnantian interval (*1*, *28*). Marine invertebrate genus diversity (black spindle) (*29*) declined both at the beginning and at the end of the Hirnantian stage. mya, million years ago.

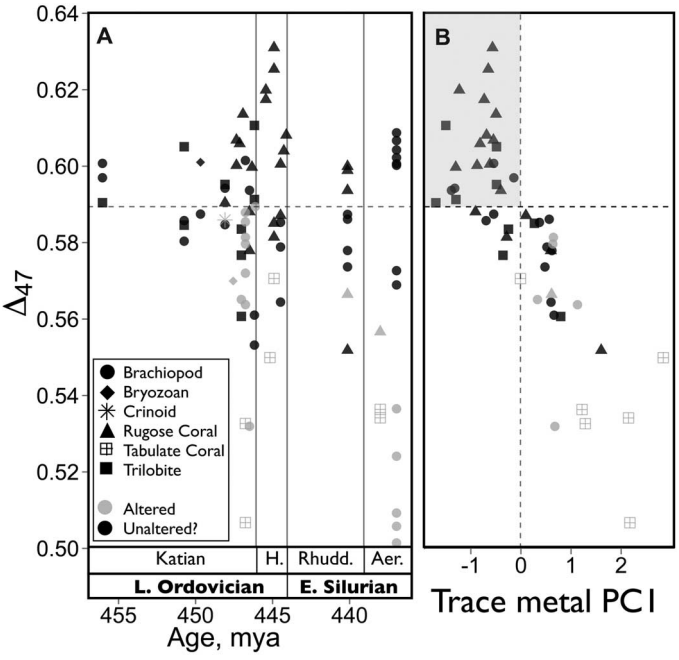

Fig. 2. (**A**) Δ_{47} values of all samples examined for this study, keyed to taxonomic group and preservation state, and plotted against stratigraphic position. (**B**) PC1 of log-transformed Mn, Fe, and Sr concentrations for a large subset ($n = 52$) of the samples shown in (A). PC1 explains 86% of variation in trace metal composition and receives strong positive loading from Mn and Fe and weak negative loading from Sr. Dashed lines indicate PC1 and Δ_{47} cutoffs for inclusion (shaded region) in paleoclimate reconstructions; H, Hirnantian; Rhudd, Rhuddanian; Aer, Aeronian. Ages within stages are interpolated on the basis of stratigraphic position.

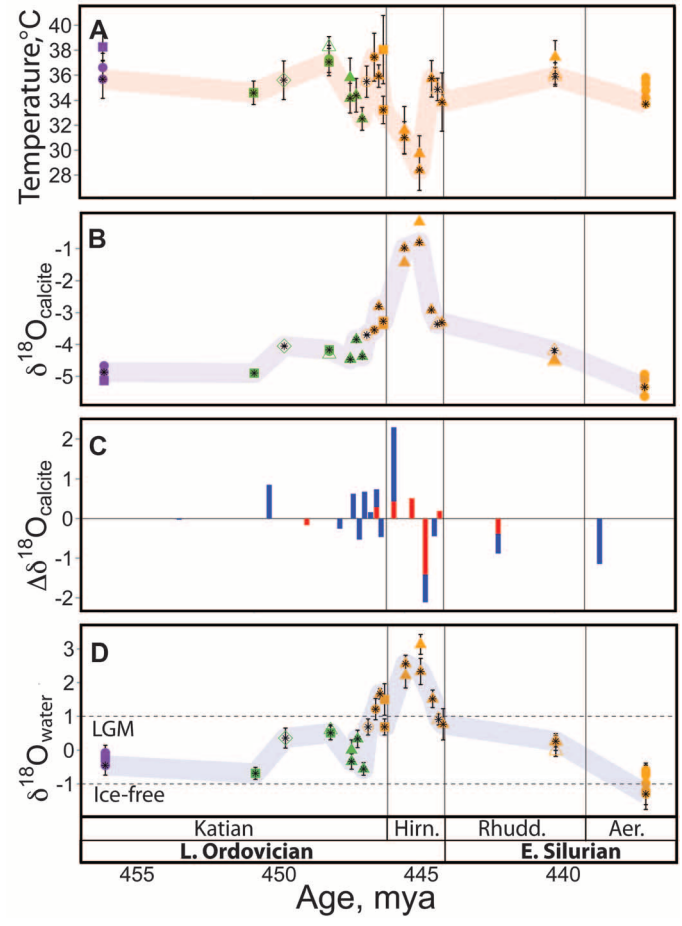

Fig. 3. Symbols as in Fig. 2; color indicates provenance: purple, Upper Mississippi Valley; green, Cincinnati Arch; orange, Anticosti Island. Solid symbols indicate samples selected on the basis of both trace metal concentration and Δ_{47} criteria; open symbols indicate samples selected based only on Δ_{47} value. Error bars on individual samples (*13*) are ± 1 SE ($\delta^{18}O$ errors are smaller than symbols) and reflect analytical precision for samples analyzed once and reproducibility for samples analyzed multiple times (table S1). Samples marked by asterisks are the lowest-temperature samples in their respective time intervals and are the basis for trendlines. (**A**) Δ_{47}-derived near-surface ocean temperature trend for the early Katian to late Aeronian interval. (**B**) $\delta^{18}O$ (VPDB) trend over the same interval. (**C**) Relative contributions of temperature and $\delta^{18}O_{water}$ to changes in $\delta^{18}O$ ($\Delta\delta^{18}O$) between successive time intervals. Bars are scaled to the magnitude of $\Delta\delta^{18}O$, and color proportion is scaled to the relative contribution of temperature change (red) and change in the oxygen isotopic composition of seawater (blue) to $\Delta\delta^{18}O$. (**D**) $\delta^{18}O_{water}$ (VSMOW) trend. Dotted lines indicate $\delta^{18}O_{water}$ value during the Pleistocene LGM (*10*) and expected $\delta^{18}O_{water}$ value for an ice-free world.

Hirnantian excursion can be defined by using only rugose corals (fig. S10) and thus cannot be explained by systematic differences between rugose corals and other taxa.

Our Δ_{47} measurements place independent constraints on how much of the temporal variation in $\delta^{18}O$ can be explained by temperature changes, with the remainder attributable to changes in the isotopic composition of seawater. For much of the study interval, $\delta^{18}O$ variation is driven almost entirely by changes in $\delta^{18}O_{water}$ (Fig. 3C); only during Hirnantian time can changes in temperature account for a substantial proportion of this variation.

$\delta^{18}O_{water}$ estimates (Fig. 3D) fall between –1‰ Vienna standard mean ocean water (VSMOW), the value expected for an ice-free world (*22*), and 1‰, the value of LGM seawater (*10*), for most of the study interval. However, $\delta^{18}O_{water}$ estimates exceed 2‰ during the Hirnantian glacial maximum. Assuming (i) the $\delta^{18}O$ trend reflects changes in mean ocean water, (ii) the $\delta^{18}O$ of all surface reservoirs combined has been unchanged from the Late Ordovician to the recent (*13*), and (iii) the $\delta^{18}O$ of glacial ice was comparable to the LGM, these values imply that continental ice volumes during the Hirnantian maximum substantially exceeded those of the LGM (fig. S11). The mean isotopic composition of Late Ordovician glacial ice cannot be directly measured, but inferred Hirnantian ice volumes exceed those of the LGM for any mean ice value heavier than –60‰, approaching the most depleted values observed in the present day (fig. S11).

$\delta^{18}O_{water}$ trends suggest multiple episodes of moderate glaciation and deglaciation throughout the mid-late Katian interval, with little evidence of substantial ice sheets before this time (Fig. 3D). The most enriched $\delta^{18}O_{water}$ values before the Himantian peak come from the sub-Laframboise Ellis Bay Formation, the age of which has been controversial (*13*). Assigning this unit an early Hirnantian rather than latest Katian age would restrict $\delta^{18}O_{water}$ values higher than 1‰ to Hirnantian time (fig. S12), but multiple mid-late Katian samples > 0‰ still indicate the development of substantial pre-Hirnantian ice sheets, at least transiently. Relatively high $\delta^{18}O_{water}$ values also occur in latest Hirnantian samples from the lowermost Becscie Formation, which records a sharp rise in sea level and waning of the Hirnantian carbon isotope excursion. These observations reveal that latest Ordovician sea level rise represents only partial deglaciation of Gondwana. $\delta^{18}O_{water}$ values consistent with moderate ice sheets persist for several million years, returning to near –1‰ by the end of the Aeronian Stage (Fig. 3D).

Our results imply that initial glaciation of Gondwana occurred with little or no cooling of the tropical oceans, that tropical SSTs exceeded the present-day range except during the Hirnantian glacial maximum, and that they warmed rapidly after the Hirnantian maximum despite the persistence of substantial continental ice volumes for several million years. This contrasts with

previous work using classical oxygen isotope paleothermometry on conodont apatite from Anticosti and elsewhere (*7*) that reconstructed temperatures in the modern SST range for much of the Late Ordovician–Early Silurian except for cooling to ~24°C below and above the Laframboise Member (*7*). These estimates assumed a constant $\delta^{18}O_{water}$ of –1.0‰; substituting our $\delta^{18}O_{water}$ values from the same units raises inferred temperatures by, on average, 8°C. Recent revision of the phosphate-water oxygen isotope fractionation equation (*23*) further suggests that all conodont-derived temperature estimates should be revised upward, bringing them into the range that we observe for the Late Ordovician–Early Silurian.

We cannot rule out the possibility that the trends we observe are influenced by changes in the basin hydrology of the Taconic Foreland, but, if they accurately reflect global trends in the tropical oceans, they imply a nonlinear relationship between tropical ocean temperatures and continental ice volumes (fig. S13A). This contrasts with expectations from climate simulations using a modern continental configuration and from proxy records of the past 60 million years (*13*) (fig. S13, B and C). Furthermore, coexistence of substantial south polar ice sheets with tropical SSTs regionally in excess of 30°C implies a steeper meridional temperature gradient than during other major glacial episodes (*12*, *24*). Minor glaciations inferred to have occurred under high CO_2 conditions in the late Mesozoic–early Cenozoic (*16*, *25*) may have exhibited similar gradients but were comparatively short-lived. Both of these observations could plausibly be explained by nonlinear changes in the intensity of oceanic meridional overturning circulation (*26*), similar to those previously invoked to explain changes in the behavior of the Hirnantian carbon cycle (*4*, *5*, *20*). Although speculative, some support for this hypothesis is provided by the coincidence of our observed cooling pulse with the globally recognized Hirnantian positive carbon isotope excursion (*5*, *19*, *20*).

Lastly, by demonstrating that tropical cooling was largely limited to the Hirnantian Stage, our results support hypotheses linking the two-pulsed nature of the Late Ordovician mass extinction to rapid climate changes at the beginning and end of this interval (*4*, *20*).

References and Notes

1. L. A. Frakes, J. E. Francis, J. I. Syktus, *Climate Modes of the Phanerozoic* (Cambridge Univ. Press, Cambridge, 1996).
2. A. Raymond, C. Metz, *J. Geol.* **112**, 655 (2004).
3. R. A. Berner, *Geochim. Cosmochim. Acta* **70**, 5653 (2006).
4. P. M. Sheehan, *Annu. Rev. Earth Planet. Sci.* **29**, 331 (2001).
5. P. J. Brenchley *et al.*, *Geology* **22**, 295 (1994).
6. D. P. Le Heron, J. A. Dowdeswell, *J. Geol. Soc. London* **166**, 277 (2009).
7. J. A. Trotter, I. S. Williams, C. R. Barnes, C. Lécuyer, R. S. Nicoll, *Science* **321**, 550 (2008).
8. J. D. Marshall, P. D. Middleton, *J. Geol. Soc. London* **147**, 1 (1990).
9. A. D. Herrmann, M. E. Patzkowsky, D. Pollard, *Palaeogeogr. Palaeoclimatol. Palaeoecol.* **206**, 59 (2004).
10. D. P. Schrag *et al.*, *Quat. Sci. Rev.* **21**, 331 (2002).
11. P. Ghosh *et al.*, *Geochim. Cosmochim. Acta* **70**, 1439 (2006).
12. R. E. Came *et al.*, *Nature* **449**, 198 (2007).
13. Materials and methods are available as supporting material on *Science* Online.
14. U. Brand, J. Veizer, *J. Sediment. Res.* **50**, 1219 (1981).
15. G. A. Shields *et al.*, *Geochim. Cosmochim. Acta* **67**, 2005 (2003).
16. A. Bornemann *et al.*, *Science* **319**, 189 (2008).
17. S. Schouten *et al.*, *Geology* **31**, 1069 (2003).
18. P. N. Pearson *et al.*, *Nature* **413**, 481 (2001).
19. A. Desrochers, C. Farley, A. Achab, E. Asselin, J. F. Riva, *Palaeogeogr. Palaeoclimatol. Palaeoecol.* **296**, 248 (2010).
20. P. J. Brenchley *et al.*, *Geol. Soc. Am. Bull.* **115**, 89 (2003).
21. L. Hints *et al.*, *Est. J. Earth Sci.* **59**, 1 (2010).
22. S. M. Savin, *Annu. Rev. Earth Planet. Sci.* **5**, 319 (1977).
23. E. Pucéat *et al.*, *Earth Planet. Sci. Lett.* **298**, 135 (2010).
24. MARGO Project Members, *Nat. Geosci.* **2**, 127 (2009).
25. A. Tripati, J. Backman, H. Elderfield, P. Ferretti, *Nature* **436**, 341 (2005).
26. R. J. Stouffer, S. Manabe, *Clim. Dyn.* **20**, 759 (2003).
27. L. R. M. Cocks, T. H. Torsvik, *J. Geol. Soc. London* **159**, 631 (2002).
28. M. R. Saltzman, S. A. Young, *Geology* **33**, 109 (2005).
29. J. J. Sepkoski Jr., *Bull. Am. Paleontol.* **363**, 560 (2002).

30. We thank T. Raub, M. Rohrssen, and B. Gaines for assistance with field and lab work; D. Boulet and Société des établissements de plein air du Québec (SEPAQ) Anticosti for permission to work in Anticosti National Park; and B. Hunda for supplying samples. This work was funded by an Agouron Institute award to W.W.F. and D.A.F. and NSF Division of Earth Sciences awards to W.W.F. and J.M.E.

Supporting Online Material

www.sciencemag.org/cgi/content/full/science.1200803/DC1
Materials and Methods
Figs. S1 to S13
Table S1
References

23 November 2010; accepted 19 January 2011
Published online 27 January 2011;
10.1126/science.1200803

Hibernation in Black Bears: Independence of Metabolic Suppression from Body Temperature

Øivind Tøien,[1]* John Blake,[1] Dale M. Edgar,[2]† Dennis A. Grahn,[3] H. Craig Heller,[3] Brian M. Barnes[1]*

Black bears hibernate for 5 to 7 months a year and, during this time, do not eat, drink, urinate, or defecate. We measured metabolic rate and body temperature in hibernating black bears and found that they suppress metabolism to 25% of basal rates while regulating body temperature from 30° to 36°C, in multiday cycles. Heart rates were reduced from 55 to as few as 9 beats per minute, with profound sinus arrhythmia. After returning to normal body temperature and emerging from dens, bears maintained a reduced metabolic rate for up to 3 weeks. The pronounced reduction and delayed recovery of metabolic rate in hibernating bears suggest that the majority of metabolic suppression during hibernation is independent of lowered body temperature.

Mammalian hibernation is well characterized in species such as marmots, ground squirrels, bats, and dasyurid marsupials (*1*). These small (<5 kg) hibernators undergo regulated decreases in core body temperature (T_b) to near or below freezing during torpor bouts that last days to weeks (*2*–*5*). Torpor is periodically interrupted by arousals to normothermia (35° to 38°C) that usually last for less than one day (*6*, *7*). During torpor, metabolic rates of small hibernators decrease to 2 to 5% of basal metabolic rate (BMR) (*8*–*10*). However, the relative contributions of temperature-dependent (described by Q_{10}, rate coefficient for a 10°C change in T_b) and temperature-independent mechanisms of metabolic suppression depend on the size of animals and stage of entry into torpor (*11*). In contrast, the relationships between T_b and metabolism in the large hibernators of the bear family Ursidae have remained unknown because technical limitations have prevented continuous, long-term monitoring in these 30 to 200 kg or larger animals. We used telemetry and respirometry to record T_b, metabolic rates, and heartbeat patterns of black bears, *Ursus americanus*, through their hibernation and post-hibernation recovery.

Black bears were nuisance animals captured in south-central or interior Alaska in late autumn 3 different years and transported to facilities at the Institute of Arctic Biology, University of Alaska Fairbanks. Radio transmitters for T_b and electromyogram (EMG)/electrocardiogram (ECG) were surgically implanted (*12*), and animals were transferred to outdoor enclosures in an isolated wooded area. Bears hibernated inside 0.8 m^3 wooden nest boxes with straw for bedding and equipped with infrared cameras, activity detectors, and telemetry-receiving antennas. Food and water were not provided. Air was continuously collected from the closed hibernacula to record O_2 consumption (a measure of metabolic rate). After

[1]Institute of Arctic Biology, University of Alaska Fairbanks, Fairbanks, AK 99775, USA. [2]Department of Psychiatry and Behavioral Sciences, School of Medicine, Stanford University, CA 94305, USA. [3]Department of Biological Sciences, Stanford University, CA 94305, USA.

*To whom correspondence should be addressed. E-mail: otoien@alaska.edu (O.T.); bmbarnes@alaska.edu (B.M.B.)
†Present address: Lilly Research Centre, Eli Lilly, Windlesham, Surrey, GU20 6PH, UK.